American Mineralogist, Volume 99, pages 1119–1126, 2014

Melting phase equilibria of model carbonated peridotite from 8 to 12 GPa in the system CaO-MgO-Al_2O_3-SiO_2-CO_2 and kimberlitic liquids in the Earth's upper mantle†

Shantanu Keshav[1,*] and Gudmundur H. Gudfinnsson[2,†]

[1]Bayerisches Geoinstitut, Universität Bayreuth, D-95440, Bayreuth, Germany
[2]Iceland GeoSurvey, 108 Reykjavik, Iceland

Abstract

Pressure-temperature divariant melting phase relations of model carbonated peridotite in the system CaO-MgO-Al_2O_3-SiO_2-CO_2 from 8 to 12 GPa are reported. From 8 to 12 GPa, melting temperatures on the studied pressure-temperature divariant surface rise quite rapidly. Liquids, in equilibrium with forsterite, orthopyroxene, clinopyroxene, and garnet, on the low-temperature side of the divariant surface are magnesiocarbonatitic in composition. With increasing temperature along an isobar on the pressure-temperature divariant surface, and with the same crystalline phase assemblage, liquids gradually become kimberlitic in their composition. Given the model system data reported here, Group IB kimberlites and perhaps some kimberlites from Greenland, Canada, and South Africa could be generated from direct melting of carbonated peridotite in the pressure range of approximately 6–8 GPa. Some kimberlites from Canada and Russia could have formed by partial melting of carbonated mantle peridotite at pressures of about 10–12 GPa. From 8 to 12 GPa, liquid compositions on the studied divariant surface show a limited compositional range, which implies that the divariant surface is essentially flat. The implied flatness of the divariant surface, and so long as the liquid is in equilibrium with the crystalline assemblage of forsterite + orthopyroxene + clinopyroxene + garnet on the divariant surface, indicate that kimberlites belonging to Group IA and those more magnesian than Group IA cannot have their origin in only being a melting product of carbonated mantle peridotite. The absence of topography of the studied pressure-temperature divariant surface in all likelihood limits the generation of kimberlites in the Earth's upper mantle only.

Keywords: Kimberlites, magma generation, carbonated peridotite, carbonatites, diamonds

Introduction

Kimberlites are carbon dioxide (CO_2)- and water (H_2O)-rich, ultrabasic, silica-undersaturated liquids (magmas/melts; Mitchell 1986, 1995; Ulmer and Sweeney 2002; Sparks 2013). Kimberlites perhaps form part of a sequence of silica-undersaturated rocks that can vary quite widely in their composition, and might include rocks as diverse as melilitites, nephelinites, and lamproites. Kimberlites that contain diamonds must have originated from depths of at least 140–150 km in the Earth (Shirey et al. 2013; Sparks 2013).

On the basis of mineralogy, geochemistry, and isotopic compositions, two broad groups of kimberlites have been identified: Group I (basaltic) kimberlites and Group II kimberlites (micaceous; sometimes also called "orangeites") in previous studies (Smith et al. 1985; Mitchell 1986, 1995; Becker and Le Roex 2006). Because the erupted kimberlites have been extensively contaminated by "foreign" material, and as there is not a single glassy (sensu stricto) erupted kimberlite, such a classification is fraught with its own set of difficulties (Mitchell 2008; Kjarsgaard et al. 2009). Yet, from rare hypabyssal and aphanitic eruptions, estimates of "primary" kimberlite magma compositions have appeared in the published literature (e.g., Kopylova et al. 2007; Kjarsgaard et al. 2009; Patterson et al. 2009 and references therein; Sparks et al. 2009).

A causal link between kimberlites and carbonatites, from direct melting of a carbonated peridotite has been suggested to exist (Wyllie and Huang 1975; Canil and Scarfe 1990; Bailey 1993; Dalton and Presnall 1998; Gudfinnsson and Presnall 2005). That is, in experimental petrologic studies, carbonatites, which are low-degree melting products, give way to kimberlites, as the degree of melting of carbonated peridotite progresses. Among the studies mentioned, the ones of Dalton and Presnall (1998) and Gudfinnsson and Presnall (2005), undertaken in the system CaO-MgO-Al_2O_3-SiO_2-CO_2 (CMAS-CO_2), demonstrate experimentally the continuum between carbonatites and kimberlites. Wyllie (1980, 1987, 1995) and Green et al. (1987) preferred a petrological scenario wherein volatiles are transferred from somewhere in the continental asthenospheric mantle to shallower depths (e.g., asthenosphere-lithosphere "boundary"), and this transfer of volatiles generates kimberlites and carbonatites. Kimberlites are not generated only from high-pressure melting of carbonated peridotite, however. For instance, Kawamoto

* Present address: Geosciences Montpellier, University of Montpellier 2, CNRS & UMR 5243, 34095 Montpellier, France. E-mail: shantanu.keshav@gm.univ-montp2.fr
† Present address: Institute of Earth Sciences, University of Iceland, 101 Reykjavik, Iceland.

0003-004X/14/0506–1119$05.00/DOI: http://dx.doi.org/10.2138/am.2014.4826

and Holloway (1997) in their study on melting phase relations of multicomponent, hydrous (water-saturated) peridotite also noticed kimberlite-like liquid compositions at the solidus at about 10–11 GPa; at lower pressures, the liquids resemble basalts and komatiites. Hence, there is experimental evidence that water-rich kimberlites could have originated from direct melting of a hydrous mantle peridotite in the deeper portions of the Earth's upper mantle.

The other approach in addressing the petrogenesis of kimberlites lies in what is called the "multiple saturation" technique. This approach forms the basis of a petrological philosophy that equilibrium should exist between a primary kimberlite and the source. That is, a primary kimberlite should saturate with a multi-phase mantle assemblage at its conditions of origin (Eggler and Wendlandt 1979; Edgar et al. 1988; Ringwood et al. 1992; Edgar and Charbonneau 1993; Girnis et al. 1995; Yamashita et al. 1995; Ulmer and Sweeney 2002; Mitchell 2004; Girnis et al. 2011; Sokol et al. 2013).

Here, we report melting phase relations of model carbonated peridotite in the system CMAS-CO_2 from 8 to 12 GPa. The objective is twofold: (1) does the earlier-proposed continuum between model carbonatites and kimberlites over 3–8 GPa (Gudfinnsson and Presnall 2005), cease to exist at and beyond 8 GPa? If so, could kimberlites be directly produced at the solidus of model carbonated peridotite at and beyond 8 GPa. This first part is relevant to consider, for, recently a model for the eruption dynamics of kimberlites was developed wherein kimberlites in natural settings were purported to start out as carbonatites; these carbonatites at various depths in the mantle assimilate mantle material (opx) upon their ascent, and become kimberlites (Russell et al. 2012). The second (2) question is could the naturally occurring kimberlites as magnesian as Group IA, and perhaps even more magnesian than this Group, be produced simply from melting of carbonated peridotite, at pressures yet greater than 10–12 GPa (Gudfinnsson and Presnall 2005)?

The intent of the present experimental work is illustrated in Figure 1 (modified after Dalton and Presnall 1998; Gudfinnsson and Presnall 2005). The present experimental study is toward the higher pressure side of the vertical, dashed line on the *P-T* divariant surface (Fig. 1). The present experimental study builds upon melting phase relations in model carbonated peridotite reported earlier (Dalton and Presnall 1998; Gudfinnsson and Presnall 2005). Besides presenting more complete data set at 8 GPa than was done in Gudfinnsson and Presnall (2005), we further explore the topology of the *P-T* divariant surface up to 12 GPa. The influence of alkalies (Na_2O and K_2O), water (H_2O), iron oxide (FeO), and titanium oxide (TiO_2), components that might have significant influence on the melting phase relations is unknown at the moment and is not considered here.

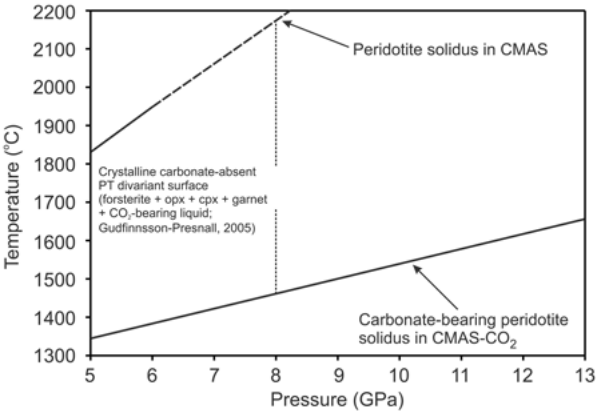

Figure 1. This pressure-temperature projection shows solidus curves for volatile-free (CaO-MgO-Al_2O_3-SiO_2; CMAS) and CMAS-CO_2 peridotite. The 5 and 6 GPa peridotite solidus data in the system CMAS are from Presnall and Gudfinnsson (2011), and is labeled "Peridotite solidus in CMAS". After 6 GPa, the solidus curve of dry, model peridotite in the system CMAS is not known, and is hence shown in thick dashed curve. The solidus curve of model, carbonated peridotite in the system CMAS-CO_2 labeled "Carbonate-bearing peridotite solidus in CMAS-CO_2" is after Dalton and Presnall (1998), Gudfinnsson and Presnall (2005), and Keshav et al. (2011). Melting phase relations of model carbonated peridotite on the *P-T* divariant surface (labeled "crystalline carbonate-absent *P-T* divariant surface") are known from 5 to about 8 GPa. The present experimental work is toward the higher pressure side of the vertical, dashed line on the *P-T* divariant surface. The vertical, dashed line has no geometrical meaning, and is drawn to only demarcate regions on the *P-T* divariant surface where there is most experimental coverage, that is between 5 and about 8 GPa (Gudfinnsson and Presnall 2005).

Method

The experiments were conducted by using starting mixtures listed in Table 1. These were prepared so as to have a large amount of liquid that is in equilibrium with a peridotite crystalline phase assemblage. This philosophy was adopted to facilitate analysis of liquids using the electron microprobe. Starting mixtures labeled *JADSCM-3*, *JADSCM-7*, *JADSCM-8*, and *JADSCM-14*, were identical to those used by Gudfinnsson and Presnall (2005), and were taken from the batches prepared by Gudfinnsson and Presnall (2005). Other starting mixtures were prepared afresh (for details, the reader is referred to the studies of Dalton and Presnall 1998 and Gudfinnsson and Presnall 2005). Briefly, all the starting compositions were prepared using a combination of shelf carbonate and oxides: $CaCO_3$ (Alfa Aesar, 99.998%), MgO (Alfa Aesar, 99.998%), Al_2O_3 (Alfa Aesar, 99.998%), and SiO_2 (Aldrich, 99.995%). Magnesite from Oberdorf (Austria; generously supplied by Peter Ulmer, ETH Zürich) provided all CO_2 and some MgO. This particular magnesite was used in the experimental work on the pseudobinary $CaCO_3$-$MgCO_3$ by Buob et al. (2006). The silicate portion of the starting mixtures was prepared first as a glass. All the components were fired in platinum (Pt) crucibles for at least 18–20 h in air: MgO, Al_2O_3, and SiO_2 at 1250 °C, and $CaCO_3$ at 400 °C. Pt crucibles were used that had not been previously utilized to dry either iron metal or iron oxides. To prepare the starting mixture, fired oxides and $CaCO_3$ were immediately mixed in appropriate proportions, and ground for at least 1 h under ethanol in an agate mortar. After drying under an infrared (IR) heat lamp, this mixture, contained in a Pt-crucible, was decarbonated in air in a box furnace. To decarbonate, temperature of the furnace was slowly ramped to 1000 °C over 10 h, and maintained at this temperature for 6–7 h. After this step, the Pt-crucible was taken out of the furnace, and then transferred to another high-temperature furnace to prepare glass by melting in air at 1650 °C for about 4 h. To quench this liquid to glass, the Pt-crucible was partially immersed in an ice-water bath, and the resulting glass was optically pure and transparent. This glass was finely ground under ethanol for about

Table 1. Nominal composition of starting mixtures in the system CMAS-CO_2 used in the present experimental study (wt%)

Mixture	CaO	MgO	Al_2O_3	SiO_2	CO_2[a]
JADSCM-3	21.36	25.68	3.04	27.54	22.82
JADSCM-7	10.95	33.38	4.02	43.15	8.50
JADSCM-8	12.48	32.76	3.31	39.21	12.24
JADSCM-14	9.74	34.20	4.90	46.57	4.59
CMAS-CO_2-24	11.44	36.99	2.17	31.17	18.24
CMAS-CO_2-26	10.22	38.77	2.09	33.83	15.09
CMAS-CO_2-29	9.43	39.68	2.32	37.65	10.92
CMAS-CO_2-30	9.49	39.65	2.74	40.25	7.87
CMAS-CO_2-32	10.11	38.29	4.09	41.16	6.36

[a] Added as crystalline magnesite, $MgCO_3$.

30–40 min, and using the same procedure, glassing was repeated once more. To ensure homogeneity, the silicate glass was re-ground for 1 h under ethanol in an agate mortar, and then dried under an IR heat lamp for about 1 h. Finely ground magnesite was fired at 200–250 °C in air in a Pt-crucible for over 17 h. Silicate glass and magnesite were mixed and ground in an agate mortar under ethanol for another 1 h, and the final contents poured in a glass vial and stored in a desiccator.

All the experiments from 8 to 12 GPa were performed in a traditional, uniaxial, split-sphere, multi-anvil apparatus (MA6/8 module; Sumitomo 1200 press; Rubie 1999; Keppler and Frost 2005) installed at Bayerisches Geoinstitut (BGI). The experiments were performed using Cr_2O_3-doped MgO pressure cells with an edge length of 14 mm. Second-stage tungsten carbide anvils (32 mm edge length) with 8 mm (Toshiba F grade) truncated edge lengths were used in the experiments. Cells in the multi-anvil press were brought to target pressures over 10–12 h, and then temperature was directly increased to the target values (Table 2). On the basis of pressure calibrations reported earlier (Keppler and Frost 2005), the pressure uncertainty in the present set of experiments is estimated to be on the order of 0.2 GPa. On the basis of two-pyroxene thermometry, the temperature gradient in the 14/8 type pressure cells used in the present study, is on the order of ±50 °C. For details regarding the rest of the experimental procedures, the reader is referred to Keshav et al. (2011). After each run, the capsule was recovered from the pressure cell, mounted longitudinally in Petropoxy-154 resin, and ground and polished for optical and electron microprobe examination. Charges were polished under water-absent conditions, using kerosene-based oil (Buehler) on SiC grit (240–1000) paper. Charges were vacuum-impregnated multiple (3–4) times with resin (Petropoxy-154). After this step, regrinding of the charges was done on SiC grit papers under kerosene-based oil (Buehler), until a satisfactory surface for oil-based diamond polishing (3–0.25 μm) was obtained.

The compositions of crystalline phases and quenched liquid were determined by wavelength-dispersive electron microprobe (5-spectrometer JEOL-JXA 8200 Superprobe at BGI) with an accelerating voltage of 15 kV and 15 nA probe current (at the Faraday cup). Quenched liquid was analyzed using a beam diameter of 3–10 μm, and the beam diameter was 1 μm for crystalline phases. The analyses were performed in a fixed spot mode, and were reduced using the ZAF correction scheme. The amount of CO_2 in liquid was calculated by difference, and the four oxides (CMAS) were measured using a combination of diopside, forsterite, pyrope, and enstatite standards.

Experiments reported here were not reversed, and hence attainment of chemical equilibrium is not proven. Lack of zoning in the crystalline phases and internally consistent liquid compositions in the experiments are consistent with near-equilibrium conditions. Liquid did not quench to glass in the present experiments. Instead, it is quenched to a fine mixture of silicate and carbonate fractions, resembling the textures reported previously (Dalton and Presnall 1998; Gudfinnsson and Presnall 2005; Keshav et al. 2011). (The presence of both silicate and carbonate fractions in the quenched materials does not imply that there are two, separate liquids, silicate and carbonate in composition.) For this reason, at least 30–45 analyses were acquired. Quenched liquid is, in some cases, segregated from rest of the crystalline mass. This effect is most likely due to temperature gradient that originates in the pressure cells employed here (also discussed in Gudfinnsson and Presnall 2005). The experimental conditions and composition of phases are shown in Table 2.

Quenched liquid compositions in the experiments

All the experiments reported here contain assemblages consisting of forsterite + opx + cpx + garnet + liquid. There is no evidence of liquid immiscibility, and hence the experiments in the present study are consistent with studies at lower pressure (Dalton and Presnall 1998; Gudfinnsson and Presnall 2005). From 8 to 12 GPa in the present experimental study, there is a gradual change in the liquid compositions, from magnesiocarbonatitic at low temperatures to kimberlitic at high temperatures with about 30–40 and 7–18 wt% dissolved CO_2, respectively (Table 2). Changes in liquid compositions, in the form of isopleths for the five oxides, are shown in Figures 2 to 6. These isopleths were sketched on the basis of liquid compositions (Table 2), and represent visual fits to the data; also shown for reference are the isopleths from Gudfinnsson and Presnall (2005). The results of the present experimental study from 8 to 12 GPa confirm the

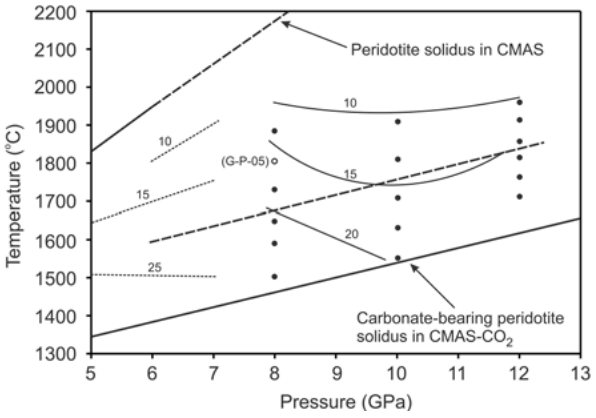

Figure 2. Isopleths for the concentrations of CaO (wt%) in the liquids, which are in equilibrium with garnet peridotite assemblage. Isopleths drawn on the basis of this study and those from Gudfinnsson and Presnall (2005) are shown in solid curves/lines and dashed lines, respectively. Number next to a particular curve/line is the concentration of CaO in the liquid. Data points from the present study are shown in dark, filled circles. One datum at 8 GPa from Gudfinnsson and Presnall (2005) is shown in open circle as "G-P-05". The thick, dashed line in this projection is the approximate boundary between carbonatites (toward lower temperatures) and kimberlites (toward higher temperatures), and is drawn here on the basis of classification scheme proposed by Woolley et al. (1996). The carbonate-bearing peridotite solidus in the system CMAS-CO_2 is drawn after Dalton and Presnall (1998), Gudfinnsson and Presnall (2005), and Keshav et al. (2011). The solidus of peridotite in the system CMAS is after Presnall and Gudfinnsson (2011).

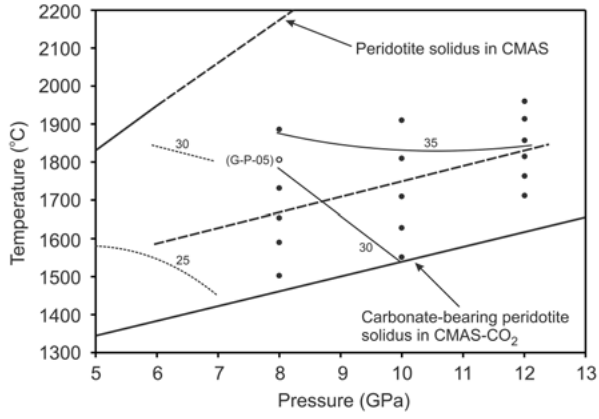

Figure 3. Isopleths for the concentrations of MgO (wt%) in the liquids, which are in equilibrium with garnet peridotite assemblage. Number next to a particular curve/line is the concentration of MgO in the liquid. Rest as in Figure 2.

continuum between carbonatites at low temperatures and model kimberlites at high temperatures, as was documented at lower pressures (Dalton and Presnall 1998; Gudfinnsson and Presnall 2005). With increasing pressure from 8 to 12 GPa, liquids on the low-temperature side of the *P-T* divariant surface become increasingly magnesian with increasing temperature, although they do not really become kimberlite in composition ("Kimberlites" in Fig. 7). We note that with increasing pressure from 8 to 12 GPa,

TABLE 2. Experimental conditions and electron microprobe analyses (wt%) of crystalline phases and quenched liquids from the experimental charges of the present study

Experiment	CaO	MgO	Al_2O_3	SiO_2	CO_2	Sum
K-1 (*JADSCM-3*)[a] – 8 GPa/1500 °C/6 h[b]						
Forsterite (15)[c] (5)[d]	0.38 (0.1)	57.22 (0.86)	0.29 (0.03)	43.44 (0.51)		101.33
Opx (9) (2)	2.67 (0.66)	38.10 (0.77)	1.59 (0.13)	57.96 (0.91)		100.32
Cpx (14) (28)	17.91(0.79)	24.05 (1.01)	1.11 (0.36)	56.89 (0.61)		99.96
Gt (6) (12)	5.79 (0.34)	28.11 (0.51)	21.92 (0.55)	45.73 (0.48)		101.55
Melt (37) (53)	25.44(2.34)	24.31 (2.21)	0.20 (0.1)	10.20 (2.43)	39.85[e]	100.00
K-3 (*JADSCM-8*) – 8 GPa/1575 °C/6 h						
Forsterite (15) (15)	0.30 (0.1)	57.14 (0.41)	0.10 (0.08)	43.38 (0.74)		100.92
Opx (11) (19)	1.96 (0.57)	37.88 (0.81)	1.99 (0.23)	57.22 (0.54)		99.05
Cpx (12) (14)	17.41(0.29)	24.63 (0.86)	1.22 (0.18)	57.01 (0.77)		100.27
Gt (4) (12)	5.55 (0.31)	27.23 (0.58)	20.88 (0.79)	45.66 (0.64)		99.32
Melt (31) (40)	21.44 (2.40)	26.11 (1.87)	0.90 (0.24)	20.77 (3.01)	30.78	100.00
K-4 (*JADSCM-7*) – 8 GPa/1650 °C/6.5 h						
Forsterite (9) (14)	0.20 (0.12)	57.21 (0.46)	0.22 (0.08)	43.20 (0.66)		100.83
Opx (10) (18)	1.55 (0.56)	37.64 (0.83)	1.39 (0.33)	58.70 (0.91)		99.28
Cpx (17) (13)	16.99 (0.42)	25.04 (0.45)	1.30 (0.22)	56.58 (0.60)		99.91
Gt (9) (14)	6.41(0.32)	26.47 (0.44)	19.93 (0.62)	46.10 (0.20)		98.91
Melt (40) (41)	20.07(1.22)	26.81 (1.69)	1.56 (0.44)	20.01 (2.88)	20.01	100.00
K-9 (*JADSCM-7*) – 8 GPa/1725 °C/6 h						
Forsterite (11) (12)	0.38 (0.11)	57.51 (0.32)	0.14 (0.03)	42.96 (0.52)		100.99
Opx (8) (18)	1.94 (0.40)	38.10 (0.70)	1.50 (0.20)	57.96 (0.33)		99.50
Cpx (10) (13)	15.93 (0.39)	27.82 (0.67)	2.01 (0.22)	55.10 (0.49)		100.86
Gt (4) (14)	6.11(0.21)	26.77 (0.55)	20.96 (0.38)	46.20 (0.66)		100.04
Melt (35) (43)	17.67 (1.22)	29.11 (2.22)	2.32 (0.81)	32.10 (2.68)	18.80	100.00
K-6 (*JADSCM-14*) – 8 GPa/1875 °C/5 h						
Forsterite (12) (4)	0.42 (0.14)	57.77 (0.46)	0.19 (0.09)	42.55 (0.40)		100.93
Opx (12) (24)	2.22 (0.33)	38.66 (0.47)	1.31 (0.31)	57.59 (0.52)		99.78
Cpx (10) (13)	13.92 (0.48)	31.33 (1.06)	1.21 (0.23)	54.84 (0.55)		101.30
Gt (4) (9)	5.17 (0.84)	27.83 (0.71)	21.11(0.67)	45.62 (0.88)		99.73
Melt (40) (50)	14.81(2.55)	35.02 (3.11)	4.93 (1.11)	36.34 (3.23)	8.60	100.00
K-10 (CMAS-CO_2-24) – 10 GPa/1550 °C/7 h						
Forsterite (8) (22)	0.28 (0.11)	57.23 (0.31)	0.10 (0.07)	42.89 (0.68)		100.50
Opx (15) (10)	3.22 (0.70)	37.17 (0.49)	0.59 (0.04)	58.11 (0.76)		99.09
Cpx (13) (9)	14.23 (0.49)	27.77 (0.40)	0.66 (0.33)	56.99 (0.59)		99.65
Gt (9) (12)	6.20 (0.31)	29.98 (0.75)	14.29 (0.88)	50.03 (0.73)		100.50
Melt (35) (47)	19.23 (2.22)	31.06 (4.01)	0.67 (0.30)	10.22 (2.99)	38.82	100.00
K-11 (CMAS-CO_2-26) – 10 GPa/1625 °C/8 h						
Forsterite (10) (25)	0.30 (0.10)	57.45 (0.55)	0.13 (0.05)	43.11 (0.70)		100.99
Opx (11) (7)	3.44 (0.56)	37.31 (0.67)	0.70 (0.29)	58.03 (0.72)		99.48
Cpx (14) (7)	13.88 (0.48)	28.11 (0.99)	0.59 (0.21)	56.67 (0.66)		99.25
Gt (6) (10)	6.45 (0.94)	29.76 (0.41)	14.30 (0.47)	50.11 (0.66)		100.62
Melt (42) (51)	16.29 (2.23)	33.21 (2.11)	1.07 (0.44)	19.77 (2.19)	29.66	100.00
K-14 (CMAS-CO_2-29) – 10 GPa/1700 °C/5 h						
Forsterite (8) (26)	0.39 (0.10)	57.56 (0.44)	0.20 (0.09)	42.34 (0.78)		100.49
Opx (11) (8)	3.31 (0.90)	38.02 (0.69)	0.66 (0.11)	57.45 (0.96)		99.44
Cpx (17) (5)	13.22 (0.69)	27.99 (0.70)	0.61 (0.43)	57.01 (0.47)		98.83
Gt (7) (9)	5.98 (0.41)	29.11(0.65)	13.89 (0.58)	51.01 (0.93)		99.99
Melt (30) (52)	15.13 (1.22)	33.97 (3.55)	1.79 (0.67)	28.11 (1.97)	21.00	100.00
K-15 (CMAS-CO_2-30) – 10 GPa/1800 °C/5 h						
Forsterite (8) (26)	0.36 (0.05)	56.97 (0.22)	0.24 (0.10)	43.26 (0.88)		100.83
Opx (9) (3)	2.98 (0.58)	38.12 (0.53)	0.70 (0.22)	57.23 (0.55)		99.03
Cpx (11) (13)	12.89 (0.39)	28.04 (0.44)	0.80 (0.49)	57.38 (0.61)		99.11
Gt (10) (3)	5.67 (0.21)	29.22 (0.25)	12.99 (0.76)	51.11 (0.66)		98.99
Melt (35) (55)	13.58 (2.17)	34.88 (2.48)	3.94 (1.09)	33.29 (3.02)	14.31	100.00

(Continued on next page)

the liquid compositions on the studied *P-T* divariant surface do not change much (Fig. 7), compared with liquid compositions at lower pressures (Gudfinnsson and Presnall 2005). Along an isobar, however, and with increasing temperature, liquids gradually become more magnesian, and also acquire more silica (SiO_2) and alumina (Al_2O_3), and get gradually depleted in CO_2, a feature similar to what was reported at lower pressure, 3–7 GPa (Dalton and Presnall 1998; Gudfinnsson and Presnall 2005).

DISCUSSION

Figure 7 shows changes in the compositions of experimentally produced quenched liquid as a function of MgO/CaO vs. SiO_2/Al_2O_3. Experimental liquids near the carbonate-bearing peridotite solidus (Fig. 7) do not become kimberlitic in composition, and, if the phase assemblage at the solidus remains that of a carbonated peridotite, liquids are also unlikely to become kimberlitic at higher pressures (Keshav et al. 2011).

Melt compositions away from the low-temperature side of the *P-T* divariant surface from 8 to 12 GPa partly extend into the field of (reconstructed) kimberlite compositions (in the area labeled as "Kimberlites;" Fig. 7) as reported in the literature (see Mitchell 1995). Provided that the components not included in this study (iron, alkalis, titanium) do not affect the melting phase relations much, the average composition of kimberlites

TABLE 2.—*CONTINUED*

Experiment	CaO	MgO	Al_2O_3	SiO_2	CO_2	Sum
K-16 (CMAS-CO_2-30) – 10 GPa/1900 °C/2 h						
Forsterite (9) (17)	0.40 (0.12)	57.15 (0.38)	0.11 (0.07)	43.22 (0.49)		100.88
Opx (15) (2)	2.71 (0.44)	37.35 (0.73)	0.81 (0.39)	57.64 (0.60)		98.51
Cpx (15) (10)	10.33 (0.51)	28.91(0.52)	0.86 (0.50)	58.11 (0.38)		98.21
Gt (5) (1)	5.83 (0.33)	29.34 (0.55)	13.01(0.61)	51.69 (0.29)		99.87
Melt (40) (70)	10.92 (3.00)	36.41(1.44)	4.66 (1.10)	36.93 (3.44)	11.08	100.00
K-17 (CMAS-CO_2-24) – 12 GPa/1700 °C/7 h						
Forsterite (8) (22)	0.38 (0.04)	56.76 (0.33)	0.14 (0.04)	42.67 (0.71)		99.95
Opx (9) (6)	2.39 (0.46)	38.11 (0.23)	0.45 (0.37)	57.83 (0.24)		98.78
Cpx (11) (9)	15.36 (0.41)	28.02 (0.55)	0.79 (0.19)	56.44 (0.50)		100.61
Gt (8) (12)	5.55 (0.33)	28.63 (0.40)	15.41(0.62)	51.01 (0.80)		100.60
Melt (40) (51)	19.03(1.88)	30.96 (3.33)	1.21 (0.42)	14.78 (4.11)	34.02	100.00
K-18 (CMAS-CO_2-26) – 12 GPa/1750 °C/6 h						
Forsterite (8) (23)	0.27 (0.11)	57.22 (0.40)	0.21 (0.09)	42.15 (0.52)		99.85
Opx (11) (6)	3.11 (0.22)	36.84 (0.39)	0.61 (0.19)	57.85 (0.11)		98.41
Cpx (13) (2)	13.96 (0.21)	28.89 (0.69)	0.64 (0.14)	57.07 (0.55)		100.56
Gt (4) (3)	5.11 (0.29)	29.41 (0.80)	13.89 (0.72)	50.73 (0.90)		99.14
Melt (35) (66)	16.88 (2.20)	33.41 (2.81)	2.84 (0.64)	25.67 (3.16)	21.20	100.00
K-19 (CMAS-CO_2-29) – 12 GPa/1800 °C/5 h						
Forsterite (11) (22)	0.40 (0.12)	57.29 (0.21)	0.34 (0.10)	42.44 (0.68)		100.47
Opx (12) (7)	2.81 (0.67)	38.59 (0.48)	0.80 (0.21)	57.45 (0.55)		99.65
Cpx (11) (3)	12.44 (0.49)	28.86 (0.60)	0.57 (0.21)	57.69 (0.88)		99.56
Gt (6) (2)	5.67 (0.55)	29.76 (0.71)	14.17 (0.68)	51.22 (0.70)		100.82
Melt (35) (66)	15.14 (2.11)	34.94 (2.69)	3.66 (1.07)	31.08 (2.77)	15.18	100.00
K-20 (CMAS-CO_2-30) – 12 GPa/1850 °C/4.3 h						
Forsterite (9) (21)	0.36 (0.12)	56.97 (0.38)	0.24 (0.07)	43.26 (0.33)		100.83
Opx (10) (3)	2.98 (0.51)	38.12 (0.55)	0.70 (0.22)	57.23 (0.70)		99.03
Cpx (18) (8)	12.89 (0.48)	28.04 (0.66)	0.80 (0.43)	57.38 (0.22)		99.11
Gt (7) (1)	5.15 (0.29)	30.11 (0.27)	12.30 (0.39)	50.88 (0.66)		98.44
Melt (40) (67)	13.61(2.49)	35.67 (2.87)	4.86 (1.01)	35.22 (2.91)	10.64	100.00
K-21 (CMAS-CO_2-32) – 12 GPa/1900 °C/3 h						
Forsterite (11) (12)	0.29 (0.11)	57.31 (0.32)	0.11 (0.03)	42.44 (0.52)		100.15
Opx (10) (5)	2.94 (0.40)	38.20 (0.70)	0.92 (0.20)	57.46 (0.33)		99.52
Cpx (15) (11)	11.88 (0.39)	29.64 (0.67)	0.61 (0.22)	57.47 (0.49)		100.86
Gt (6) (4)	6.33 (0.21)	30.10 (0.55)	12.27 (0.38)	52.06 (0.66)		100.76
Melt (45) (68)	12.30 (2.30)	36.81 (2.14)	5.10 (1.41)	36.44 (2.50)	9.35	100.00
K-24 (CMAS-CO_2-32) – 12 GPa/1950 °C/1.5 h						
Forsterite (9) (6)	0.39 (0.09)	56.33 (0.40)	0.09 (0.07)	43.24 (0.24)		100.05
Opx (8) (2)	3.40 (0.51)	37.33 (0.66)	1.20 (0.31)	57.11 (0.51)		99.04
Cpx (13) (13)	9.10 (0.63)	31.22 (0.81)	1.01 (0.11)	57.84 (0.67)		99.17
Gt (8) (2)	6.60 (0.32)	31.20 (0.70)	11.43 (0.44)	52.01 (0.58)		101.24
Melt (45) (77)	10.31 (2.91)	38.11 (1.67)	5.92 (0.73)	38.10 (2.91)	7.56	100.00

[a] In parentheses is the starting composition used.
[b] Run conditions in pressure, temperature, and duration.
[c] In first parentheses are the number of analyses.
[d] In second parentheses is phase proportion by weight.
[e] CO_2 in melt calculated by difference.

from Kimberley, South Africa (Clement 1982; shown as "Ki" in Fig. 7) is consistent with an origin at about 8 GPa. Equally, kimberlites of Group IB (Smith et al. 1985; shown as "1B" in Fig. 7), those of Majuagaa, Greenland (Nielsen and Jensen 2005; shown as "G" in Fig. 7), and the high-titanium kimberlites of Lac de Gras, Canada (Kjarsgaard et al. 2009; shown as "C-2" in Fig. 7) may have originated at pressures of about 6–7 GPa. Kimberlites at Jericho, Canada (Kopylova et al. 2007; shown as "J" in Fig. 7), those at Udachnaya-East (Kamenetsky et al. 2007; shown as "U" in Fig. 7), and the low-titanium kimberlites of Lac de Gras, Canada (Kjarsgaard et al. 2009; shown as "C-1" in Fig. 7) appear to have come from the highest pressures of about 10–12 GPa. If, however, the assertion of Kjarsgaard et al. (2009), that Kamenetsky et al. (2007) in arriving at a "primary" kimberlite magma composition at Udachnaya-East have incorrectly estimated the concentrations of water and carbon dioxide from the erupted kimberlites, is taken at its face value, then there are two implications: (1) it would make understanding the origin of Udachnaya-East kimberlites in the light of melting phase relations presented either here or elsewhere in the published literature extremely difficult, and (2) the low-titanium kimberlites of Lac de Gras, Canada (Kjarsgaard et al. 2009; shown as "C-1" in Fig. 7) will become the only ones to have come from the highest pressure of about 12 GPa. The kimberlites of Group IA (Smith et al. 1985; shown as "IA" in Fig. 7) are very far from the highest pressure datum investigated here (12 GPa), and from what we know in the model system CMAS-CO_2, it is unlikely that they could have their origin simply from melting of carbonated mantle peridotite at pressures less than that of about 18–20 GPa (see below). On the other hand, the reconstructed kimberlite at Wesselton, South Africa (Sparks et al. 2009; shown as "WR" in Fig. 7) indicates pressure of origin at about 4 GPa, making it the shallowest kimberlite among those considered here.

There are other kimberlitic compositions, which are even more magnesian than those of Group IA, and some of these, the so-called "contamination-free kimberlites" (Mitchell 1986), occupy roughly half the field of some "Kimberlites" shown in Figure 7 (also see Fig. 5 of Gudfinnsson and Presnall 2005). On

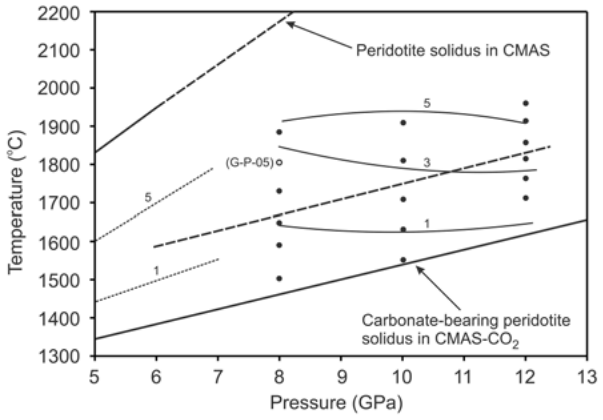

FIGURE 4. Isopleths for the concentrations of Al_2O_3 (wt%) in the liquids, which are in equilibrium with garnet peridotite assemblage. Number next to a particular curve/line is the concentration of Al_2O_3 in the liquid. Rest as in Figure 2.

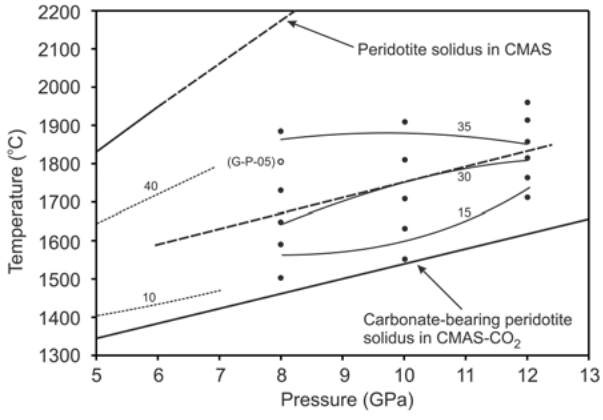

FIGURE 5. Isopleths for the concentrations of SiO_2 (wt%) in the liquids, which are in equilibrium with garnet peridotite assemblage. Number next to a particular curve/line is the concentration of SiO_2 in the liquid. Rest as in Figure 2.

the basis of data from 8 to 12 GPa we argue that the influence of increasing pressure beyond 12 GPa, on the liquid compositions on the *P-T* divariant surface, would be minimal. This is because the liquid compositions on the *P-T* divariant surface show the largest compositional range over the pressure range of 3–8 GPa, as seen in the widely spaced isobars (and oxide-ratio isopleths) that traverse this surface (Fig. 7). Given these observations, Group 1A and kimberlites more magnesian than those of Group 1A at pressures beyond 12 GPa could not have simply come from melting of carbonated peridotite. Therefore, melting phase relations in the system CMAS-CO_2, especially the closely stacked nature of oxide-ratio isopleths from 8 to 12 GPa (Fig. 7) limits the generation of kimberlites most likely in the Earth's upper mantle. If the genesis of kimberlites is indeed restricted to upper mantle depths in Earth, then how does one account for the transport of "deep" Transition Zone and even deeper "lower mantle" assemblages in diamonds to the surface of the Earth?

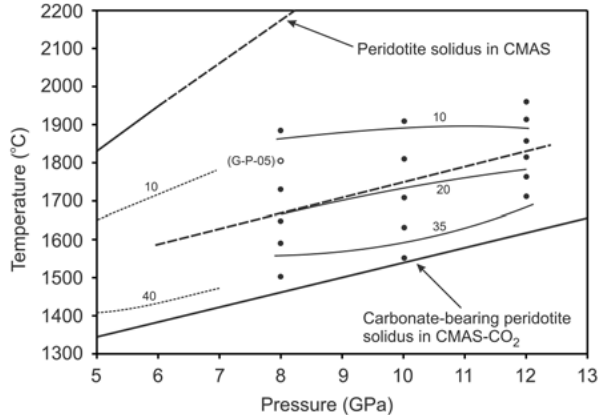

FIGURE 6. Isopleths for the concentrations of CO_2 (wt%) in the liquids, which are in equilibrium with garnet peridotite assemblage. Number next to a particular curve/line is the concentration of CO_2 in the liquid. Rest as in Figure 2.

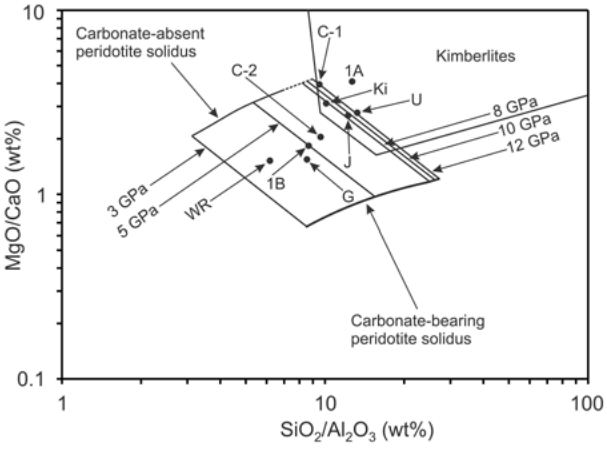

FIGURE 7. Kimberlite compositions in the form of MgO/CaO vs. SiO_2/Al_2O_3 (wt% ratios), after Rock (1991). The 3 and 5 GPa isobars have been taken directly from Gudfinnsson and Presnall (2005), while those at 8, 10, and 12 GPa are from the work presented in this manuscript. The low-temperature part of the *P-T* divariant surface, inclusive of Gudfinnsson and Presnall (2005) work, labeled "carbonate-bearing peridotite solidus" in the system CMAS-CO_2, is shown as thick, solid curve. The high temperature bound on the *P-T* divariant surface, labeled as "carbonate-absent peridotite solidus" in the system CMAS is directly taken from Gudfinnsson and Presnall (2005), and over the pressure range of 3–6 GPa, is shown as thin, solid curve; in the absence of data at pressures greater than 6 GPa, the "carbonate-absent peridotite solidus" is shown in dashed. Kimberlite compositions shown as "Ki" are from Clement (1982), and average compositions of Group IA and Group IB kimberlites are from Smith et al. (1985). The field of "Kimberlites" is after Mitchell (1986) and Mitchell (1995). Kimberlites of Majuagaa, Greenland ("G"), Jericho, Canada ("J"), Udachnaya-East ("U"), Wesselton, South Africa ("WR" = Wesselton reconstructed) are from Nielsen and Jensen (2005), Kopylova et al. (2007), Kamenetsky et al. (2007), and Sparks et al. (2009), respectively. The high-titanium kimberlites ("C-2") and low-titanium kimberlites ("C-1") are from Lac de Gras, Canada (Kjarsgaard et al. 2009).

Such assemblages have been described in diamonds from localities in Brazil, Canada, Guinea, South Africa, Venezuela, and perhaps from localities in Zimbabwe and Tanzania (Hayman et al. 2005 and references therein; Kaminsky 2012 and references therein). This transport of "deep" diamonds could occur via mantle flow from greater to shallower depths; from such depths later kimberlites could carry such diamonds and their enclosed inclusions, and bring them to the surface of the Earth.

In summary, natural kimberlites (hydrous and carbonated), could likely have their origin in one of the following ways: (1) carbonated and hydrous kimberlites in general, and those belonging to Groups IA and IB, begin as dry carbonatites, and gain water somewhere during their ascent in the Earth's upper mantle or at very shallow depths in the Earth's crust; (2) kimberlites begin as wet (water-saturated?) carbonatites, and these carbonatites somehow "donate" water to liquids that eventually are called kimberlites, or (3) kimberlites are simply the low-degree melting products of some sort of a hydrated mantle at high pressures (Kawamoto and Holloway 1997), and eventually become carbonated as they rise through the mantle column. (4) The initial melts at the solidus of carbonated peridotite are carbonatite-like; but one possibility might be that the mantle rises and follows an adiabat (or close), so the (still very low-degree) melt eventually becomes kimberlitic, before it segregates and erupts.

Implications

One of the aspects to come from the present experimental investigation is the finding that isopleths along individual isobars in oxide-ratio diagram are closer together to each other than at lower pressures in the same system, CaO-MgO-Al_2O_3-SiO_2-CO_2 (CMAS-CO_2). This observation (Fig. 7) suggests that from 8 to 12 GPa, liquid compositions do not change much, than is the case at lower pressures (Gudfinnsson and Presnall 2005). On the basis of the nature of isopleths (Fig. 7), it would seem that to achieve even a further peripheral change in liquid compositions (and so long as liquids are held in equilibrium with the four-phase assemblage of forsterite, orthopyroxene, clinopyroxene, garnet), a fairly large increase in pressure could be required. Yet, at pressures of 14–16 GPa, orthopyroxene would disappear from the carbonated mantle peridotite composition space (Keshav et al. 2011), and hence the liquid will only be in equilibrium with forsterite (or one of its polymorphs, wadsleyite/ringwoodite), clinopyroxene, and garnet. This loss of orthopyroxene from the studied composition space would increase the variance by 1; the compositions of such liquids in equilibrium with rest of the peridotite crystalline phase assemblage are not known at the moment, but should be a subject of interest because of their potential significance for primary kimberlite-like liquids at pressures corresponding to those of Earth's Transition Zone (14–22 GPa).

Additionally, in this study we have focused on the systematic evaluation of melting phase relations only of carbonated peridotite, which encompasses a fairly limited composition space in the system CMAS-CO_2. Systematic investigation of fusion relations on pressure-temperature divariant surfaces in other composition spaces, for instance, in broadly carbonated basalt or mixed lithologies (carbonated basalt-carbonated peridotite) would also be important. Likewise, within the model carbonated peridotite composition space, a methodical study of the influence of other components, especially of water, iron oxide, and perhaps alkalies, would be worthwhile. Such studies have the potential to clarify further the causal relationship between carbonatites and kimberlites in the Earth's mantle.

Acknowledgments

For discussions on the petrogenesis of carbonatites and kimberlites, the authors thank Hans Keppler, Davide Novella, and Dean Presnall. On different occasions Steven Foley, Roger Mitchell, Michael Walter, a referee who wished to remain anonymous, Journal Associate Editor Bjørn Mysen, and Journal Editor Keith Putirka officially reviewed this manuscript, and are thanked for their comments. Roger Mitchell, Bjørn Mysen, Keith Putirka, and Michael Walter are acknowledged for their tough reviews that considerably improved the contents of this manuscript. We thank our technical and administrative colleagues in France, Germany, and Iceland for their assistance. Bayerisches Geoinstitut, Germany and partial support from the 7th framework CIG Marie-Curie EU grant (303301) to the first author supported the present research.

References cited

Bailey, D.K. (1993) Carbonate magmas. Journal of the Geological Society, London, 150, 637–651.

Becker, M., and Le Roex, A.P. (2006) Geochemistry of South African on- and off-craton, Group I and Group II kimberlites: Petrogenesis and source region evolution. Journal of Petrology, 47, 673–703.

Buob, A., Luth, R.W., Schmidt, M.W., and Ulmer, P. (2006) Experiments on $CaCO_3$-$MgCO_3$ solid solutions at high pressure and temperature. American Mineralogist, 91, 435–440.

Canil, D., and Scarfe, C.M. (1990) Phase relations in peridotite + CO_2 systems to 12 GPa: Implications for the origin of kimberlite and carbonate stability in the Earth's upper mantle. Journal of Geophysical Research, 95, 15805–15816.

Clement, C.R. (1982) A comparative geological study of some major kimberlite pipes in the northern Cape and Orange Free State. Ph.D. thesis, University of Cape Town, South Africa.

Dalton, J.A., and Presnall, D.C. (1998) The continuum of primary carbonatitic-kimberlitic melt compositions in equilibrium with lherzolite: Data from the system CaO-MgO-Al_2O_3-SiO_2-CO_2 at 6 GPa. Journal of Petrology, 39, 1953–1964.

Edgar, A.D., and Charbonneau, H.E. (1993) Melting experiments on a SiO_2-poor aphanitic kimberlite from 5–10 GPa and their bearing on source of kimberlite magmas. American Mineralogist, 75, 132–142.

Edgar, A.D., Arima, M., Baldwin, D.K., Bell, D.R., Shee, S.R., Skinner, M.W., and Walker, E.C. (1988) High-pressure, high-temperature melting experiments on a SiO_2-poor aphanitic kimberlite from the Wesselton Mine, Kimberley, South Africa. American Mineralogist, 73, 524–533.

Eggler, D.H., and Wendlandt, R.F. (1979) Experimental studies on the relationship of kimberlite magmas and partial melting of peridotite. In F.R. Boyd and H.O. Meyer, Eds., 2nd International Kimberlite Conference, p. 330–338, extended abstracts. American Geophysical Union, Washington, D.C.

Girnis, A.V., Brey, G.P., and Ryabchikov, I.D. (1995) Origin of group IA kimberlites: Fluid-saturated melting experiments at 45-55 kbar. Earth and Planetary Science Letters, 134, 283–296.

Girnis, A.V., Bulatov, V.K., and Brey, G.P. (2011) Formation of primary kimberlite melts—constraints from experiments at 6–12 GPa and variable CO_2/H_2O. Lithos, 127, 401–413.

Green, D.H., Falloon, T.J., and Taylor, W.J. (1987) Mantle-derived magmas—Roles of variable source peridotite and variable C-H-O fluid compositions. In B.O. Mysen, Ed., Magmatic Processes: Physicochemical principles, vol. 1, p. 139–154. Geochemical Society, St. Louis.

Gudfinnsson, G.H., and Presnall, D.C. (2005) Continuous gradations among primary carbonatitic, kimberlitic, melilitic, basaltic, picritic, and komatiitic melts in equilibrium with garnet lherzolite at 3–8 GPa. Journal of Petrology, 46, 1645–1659.

Hayman, P.C., Kopylova, M.G., and Kaminsky, F.V. (2005) Lower mantle diamonds from Rio Siroso (Juina Area, Mato Grosso, Brazil). Contributions to Mineralogy and Petrology, 149, 430–445.

Kamenetsky, V.S., Kamenetsky, M.B., Sharygin, V.V., Faure, K., and Golovin, A.V. (2007) Chloride and carbonate immiscible liquids at the closure of the kimberlite magmas evolution (Udachnaya-East kimberlite, Siberia). Chemical Geology, 237, 384–400.

Kaminsky, F.V. (2012) Mineralogy of the lower mantle: a review of 'super-deep' mineral inclusions in diamond. Earth Science Reviews, 110, 127–147.

Kawamoto, T., and Holloway, J. (1997) Melting temperature and partial melt chemistry of H_2O-saturated mantle peridotite to 11 Gigapascals. Science, 276, 240–243.

Keppler, H., and Frost, D.J. (2005) Introduction to minerals under extreme conditions. In Miletich, R., Ed., Mineral Behaviour at Extreme Conditions, 7, p. 1–30. EMU Notes in Mineralogy, Eötvös University Press, Budapest.

Keshav, S., Gudfinnsson, G.H., and Presnall, D.C. (2011) Melting phase relations

of simplified carbonated peridotite in the systems CaO-MgO-SiO_2-CO_2 and CaO-MgO-Al_2O_3-SiO_2-CO_2: Highly calcic magmas in the Transition Zone of the Earth. Journal of Petrology, 52, 2265–2291.

Kjarsgaard, B., Pearson, D.G., Tappe, S., Nowell, G.M., and Dowall, D.P. (2009) Geochemistry of hypabyssal kimberlites from Lac de Gras, Canada: Comparisons to global database and applications to the parent magma problem. Lithos, 112S, 236–248.

Kopylova, M.G., Matveev, S., and Raudsepp, M. (2007) Searching for parental kimberlite melt. Geochimica et Cosmochimica Acta, 71, 3616–3629.

Mitchell, R.H. (1986) Kimberlites: Mineralogy, Geochemistry, and Petrology. Plenum, New York.

——— (1995) Kimberlites, Orangeites, and Related Rocks. Plenum, New York.

——— (2004) Experimental studies at 5–12 GPa of the Ondermatjie hypabyssal kimberlite. Lithos, 76, 551–564.

——— (2008) Petrology of hypabyssal kimberlites: relevance to primary magma compositions. Journal of Volcanology and Geothermal Research, 174, 1–8.

Nielsen, T.F.D., and Jensen, S.M. (2005) The Majuagaa kimberlite dyke, Maniitsoq, southern West Greenland. Geological Survey of Greenland and Denmark, Report 2005/43.

Patterson, M., Francis, D., and McCandless, T. (2009) Kimberlites: magmas or mixtures? Lithos, 112S, 191–200.

Presnall, D.C., and Gudfinnsson, G.H. (2011) Oceanic volcanism from the Low-velocity Zone—without mantle plumes. Journal of Petrology, 52, 1533–1546.

Ringwood, A.E., Kesson, S.E., Hibberson, W., and Ware, N. (1992) Origin of kimberlites and related magmas. Earth and Planetary Science Letters, 113, 521–538.

Rock, N.M.S. (1991) Lamprophyres. Blackie, Glasgow.

Rubie, D.C. (1999) Characterizing the sample environment in multi-anvil high-pressure experiments. Phase Transitions, 68, 431–451.

Russell, J.K., Porritt, L.A., Lavalle, Y., and Dingwell, D.B. (2012) Kimberlite ascent by assimilation fueled buoyancy. Nature, 481, 352–356.

Shirey, S.B., Cartigny, P., Frost, D.J., Keshav, S., Nestola, F., Nimis, P., Pearson, D.G., Sobolev, N.V., and Walter, M.J. (2013) Diamonds and mantle geodynamics. In R.M. Hazen, A.P. Jones, and J.A. Baross, Eds., Carbon in Earth, 75, p. 355–421. Reviews in Mineralogy and Geochemistry, Mineralogical Society of America, Chantilly, Virginia.

Smith, C.B., Gurney, J.J., Barton, E.S., and Bristow, J.W. (1985) Geochemical character of southern African kimberlites: A new approach based on isotopic constraints. Transactions of Geological Society of South Africa, 88, 267–280.

Sokol, A.G., Kupriyanov, I.N., Palyanov, Y.N., Kruk, A.N., and Sobolev, N.V. (2013) Melting experiments on the Udachnaya kimberlite at 6.3–7.5 GPa: implications for the role of H_2O in magma generation and formation of hydrous olivine. Geochimica et Cosmochimica Acta, 101, 133–155.

Sparks, R.S.J. (2013) Kimberlite volcanism. Annual Review of Earth and Planetary Sciences, 41, 497–528.

Sparks, R.S.J., Brooker, R.A., Field, M., Kavanagh, J., Schumacher, J.C., Walter, M.J., and White, J. (2009) The nature of erupting kimberlite melts. Lithos, 112S, 429–438.

Ulmer, P., and Sweeney, R. (2002) Generation and differentiation of group II kimberlites: constraints from a high-pressure experimental study to 10 GPa. Geochimica et Cosmochimica Acta, 66, 2139–2153.

Woolley, A.R., Bergman, S.C., Edgar, A.D., Le Bas, M.J., Mitchell, R.H., Rock, N.M.S., and Scott Smith, B.H. (1996) Classification of lamprophyres, lamproites, kimberlites, and the kalsilitic, melilititic, and leucitic rocks. Canadian Mineralogist, 34, 175–186.

Wyllie, P.J. (1980) The origin of kimberlite. Journal of Geophysical Research, 85, 6902–6910.

——— (1987) The genesis of kimberlites and some low-SiO_2, high alkali magmas: Geological Society of Australia Special Publication 14. In J. Ross, Ed., Kimberlites and Related Rocks, p. 603–615. Blackwell for the Geological Society of Australia.

——— (1995) Experimental petrology of upper mantle materials, processes, and products. Journal of Geodynamics, 20, 429–468.

Wyllie, P.J., and Huang, W.-L. (1975) Influence of mantle CO_2 in the generation of carbonatites and kimberlites. Nature, 257, 297–299.

Yamashita, H., Arima, M., and Ohtani, E. (1995) High-pressure melting experiments on Group II kimberlite up to 8 GPa: Implications for mantle metasomatism. Proceedings of the International Kimberlite Conference, 6, 669–671.

Manuscript received June 20, 2013
Manuscript accepted December 13, 2013
Manuscript handled by Bjorn Mysen